*materials*

MDPI

*Article*

# Low-Temperature Sintering of $Bi(Ni_{0.5}Ti_{0.5})O_3$-$BiFeO_3$-$Pb(Zr_{0.5}Ti_{0.5})O_3$ Ceramics and Their Performance

**Wuyang Wang [1], Shihao Wang [2], Jun Sun [2], Qiushi Wang [2] and Bijun Fang [2,*]**

[1] Bell Honors School, Nanjing University of Posts and Telecommunications, Nanjing 210023, China; q20010103@njupt.edu.cn

[2] School of Materials Science and Engineering, Jiangsu Collaborative Innovation Center of Photovolatic Science and Engineering, Jiangsu Province Cultivation Base for State Key Laboratory of Photovoltaic Science and Technology, National Experimental Demonstration Center for Materials Science and Engineering, Changzhou University, Changzhou 213164, China; a815305547@163.com (S.W.); s21010856082@smail.cczu.edu.cn (J.S.); s21010856057@smail.cczu.edu.cn (Q.W.)

* Correspondence: fangbj@cczu.edu.cn; Tel./Fax: +86-519-86330095

**Abstract:** A low-temperature sintering strategy was realized for preparing $0.21Bi(Ni_{0.5}Ti_{0.5})O_3$-$0.05BiFeO_3$-$0.74Pb(Zr_{0.5}Ti_{0.5})O_3$ (0.21BNT-0.05BF-0.74PZT) ceramics by conventional ceramic processing by adding low melting point $BiFeO_3$ and additional sintering aid $LiBO_2$. Pure perovskite 0.21BNT-0.05BF-0.74PZT ceramics are prepared at relatively low sintering temperatures, and their structure presents tetragonal distortion that is affected slightly by the sintering temperature. The 1030 °C sintered samples have high densification accompanied by relatively large grains. All ceramics have excellent dielectric performance with a relatively high temperature of dielectric constant maximum, and present an apparent relaxation characteristic. A narrow sintering temperature range exists in the 0.21BNT-0.05BF-0.74PZT system, and the 1030 °C sintered 0.21BNT-0.05BF-0.74PZT ceramics exhibit overall excellent electrical performance. The high-temperature conductivity can be attributed to the oxygen vacancies' conduction produced by the evaporation of Pb and Bi during sintering revealed by energy dispersive X-ray measurement.

**Keywords:** $Bi(Ni_{0.5}Ti_{0.5})O_3$ end component; sintering aid; sintering temperature; relaxation behavior; electrical performance



**Citation:** Wang, W.; Wang, S.; Sun, J.; Wang, Q.; Fang, B. Low-Temperature Sintering of $Bi(Ni_{0.5}Ti_{0.5})O_3$-$BiFeO_3$-$Pb(Zr_{0.5}Ti_{0.5})O_3$ Ceramics and Their Performance. *Materials* **2023**, *16*, 3459. https://doi.org/10.3390/ma16093459

Academic Editors: Jörg Wallaschek, Mickaël Lallart, Guylaine Poulin-Vittrant and Hélène Debeda

Received: 24 March 2023
Revised: 18 April 2023
Accepted: 27 April 2023
Published: 28 April 2023



## 1. Introduction

Due to the rapid development of science and technology, high-Curie-temperature ($T_C$) piezoelectric materials are required urgently because of the severe and harsh operation conditions in the application fields such as metallurgy, petroleum exploration, aeronautics and astronautics, and so on [1]. As piezoelectric ceramics are used extensively world-wide, $Pb(Zr_{1-x}Ti_x)O_3$-based (PZT) ceramics cannot meet such strict application requirements since the commercially used PZT5H ceramics have just a typical $T_C$ of 193 °C [2]. The $T_C$ temperature is rather low for application in such circumstances since piezoelectric materials are faced with an obsession of depolarization and the safe working temperature is normally far less than their $T_C$ temperature [3,4]. Therefore, developing high-$T_C$ piezoelectric materials with a large energy density to replace the PZT-based piezoceramics has become an increasingly researched hotspot in recent years [5].

As well as consideration of the operating temperature, designing the composition is very important since electrical performance is determined mainly by the composition of the piezoelectric materials. Discovering the morphotropic phase boundary (MPB) is still an important strategy to develop novel piezoelectric materials since PZT exhibits enhanced electrical performance with composition approaching the MPB [6], which is also applicable to other ferroelectric systems [7]. The improved phase structure and physical properties

are normally correlated with the coexistence of multiferroelectric phases, and further study has discovered intermediate bridge ferroelectric phases with lower symmetry [8,9].

Among versatile ferroelectrics, a $LiNbO_3$ single crystal has a high $T_C$ of 1210 °C, but its piezoelectricity is too poor and crystal growth is complex and expensive. $BiScO_3$ ceramics have a high production cost, and a $Bi(Ni_{1/2}Ti_{1/2})O_3$-based system has a difficult preparation process as discussed in our previous research [10]. The combination of Bi and $(Ni_{1/2}Ti_{1/2})$ induces our interest. $Bi(Me)O_3$, where Me can be a single trivalent ion such as In, Yb, Sc, etc., can also be our considered complex ions combination such as $Ni_{1/3}Nb_{2/3}$, $Zn_{1/2}Ti_{1/2}$, $Mg_{1/2}Zr_{1/2}$, etc., and its complex perovskite solid solution with $PbTiO_3$ was reported by Eitiel et al. [11]. Such a result promoted the research of similar systems, and MPB composition and excellent piezoelectricity in binary $Bi(Ni_{1/2}Zr_{1/2})O_3$-$PbTiO_3$ and $Bi(Ni_{0.5}Ti_{0.5})O_3$-$PbTiO_3$ were reported thereafter [12,13]. Then, ternary system $BiScO_3$-$Bi(Ni_{1/2}Zr_{1/2})O_3$-$PbTiO_3$ was reported by Zhao et al., which presents a rather large piezoelectric constant $d_{33}$ of 480 pC/N and a high $T_C$ of 439 °C [14].

Based on these research studies, a pseudo-ternary system was constructed in this work, where $Bi(Ni_{0.5}Ti_{0.5})O_3$ (BNT) was selected as one end component, which has a perovskite structure with a B-site occupied by equivalent $Ni^{2+}$ and $Ti^{4+}$ ions [15], and $Pb(Zr_{0.5}Ti_{0.5})O_3$ was selected as another end component, which can stabilize the perovskite structure more effectively than $PbTiO_3$. Ji et al. devised a pseudo-binary system $xBi(Ni_{1/2}Ti_{1/2})O_3$-$(1-x)Pb(Zr_{1/2}Ti_{1/2})O_3$ (xBNT-(1−x)PZT), in which preparation feasibility and MPB-dependent electrical properties were studied, and the 0.25BNT-0.75PZT ceramics presented excellent performance with $d_{33}$ = 510 pC/N and $T_C$ = 227 °C [16], consistent with the design of this composition. The third end component selected was $BiFeO_3$ (BF), substituting out $BiScO_3$ due to the consideration of raw material cost. Furthermore, BF presents multiferroic performance with a high $T_C$ of 810 °C, which has large theoretical saturation polarization but cannot normally be acquired due to preparation difficulty and large leakage conductivity [17]. Although pure BF ceramics were hard to prepare, BF could facilitate ceramics preparation, promote grain growth and increase densification process due to its low melting point of 930 °C, and it had many application instances [18,19]. A similar sintering aid characteristic is used to facilitate the preparation of $Bi(Ni_{0.5}Ti_{0.5})O_3$-$BiFeO_3$-$Pb(Zr_{0.5}Ti_{0.5})O_3$ (BNT-BF-PZT) ceramics in this work.

In materials science, composition, structure, performance and application have complicated mutual interactions [20], among which composition designing and ceramics processing are very important influencing factors. In this work, $0.21Bi(Ni_{0.5}Ti_{0.5})O_3$-$0.05BiFeO_3$-$0.74Pb(Zr_{0.5}Ti_{0.5})O_3$ (0.21BNT-0.05BF-0.74PZT) was chosen due to the comprehensive consideration of its performance and preparation feasibility based on the analysis of the reported ternary phase diagram and preliminary experimental study [13,16,21]. Among ceramics processing, sintering conditions are the most important factors since the phase structure, point defects, grain size, density, etc., are affected greatly by the sintering temperature and soaking time, especially for the difficult to prepare Pb- and Bi-containing ceramics [22]. Therefore, a low-temperature sintering strategy was realized due to the low melting point of BF [19] and PbO accompanied by the adding of an additional sintering aid, $LiBO_2$ [23], and the systematic influences on structure, performance and conduction mechanism were studied in detail.

## 2. Experimental Procedure

$0.21Bi(Ni_{0.5}Ti_{0.5})O_3$-$0.05BiFeO_3$-$0.74Pb(Zr_{0.5}Ti_{0.5})O_3$ (0.21BNT-0.05BF-0.74PZT) ceramics were prepared by conventional ceramic processing via low-temperature sintering technique with additional adding 0.5 wt% $LiBO_2$ as sintering aid. Well-mixed stoichiometrically weighted raw materials of $Bi_2O_3$ (>99%), NiO (>99%), $TiO_2$ (>98.5%), $Fe_2O_3$ (>99.9%), PbO (>99%) and $ZrO_2$ (>99%) were calcined at 850 °C for 2 h to obtain perovskite structure 0.21BNT-0.05BF-0.74PZT precursor powder. Sintering aid was added into the well-ground precursor powder, then, pelletization with addition of 5 wt% polyvinyl alcohol aqueous solution and formed by cold-pressing at 300 MPa were undertaken. After separate debinding

at 550 °C for 30 min, the green discs were sintered between 1010 °C and 1050 °C with 10 °C temperature interval covered by the calcined precursor powder. Detailed preparation procedure can be seen elsewhere for preparing the $0.55Bi(Ni_{0.5}Ti_{0.5})O_3$-$0.05BiFeO_3$-$0.4PbTiO_3$ system [21].

Phase structure evolution of the polished 0.21BNT-0.05BF-0.74PZT ceramics was characterized by Rigaku D/max-2500/PC X-ray Diffractometer (XRD, Tokyo, Japan) in continuous scanning mode, where the measurement 2θ range was 10–80°, step interval was 0.02° and scanning speed was 4°/min. Ceramics' free surface morphology was observed by JEOL JSM-IT100 InTouchScope™ scanning electron microscope (SEM, Tokyo, Japan) using 800 °C thermal etched 30 min samples. Silver electrode was formed by firing silver paste at 810 °C for 10 min for electrical properties' measurement. The dielectric performance–temperature relationship and impedance spectra at elevated temperatures were measured by Partulab HDMS-1000 connected with Microtest 6630-10 Precision LCR Meter (Wuhan, China). Piezoelectric constant and electromechanical coupling performance were measured by ZJ-3AN quasi-static $d_{33}$ tester (Beijing, China) and TH2826 impedance analyzer (Changzhou, China), respectively, using room-temperature poled samples in silicone oil for 1 min [21].

## 3. Results and Discussion

### *3.1. Structure and Density Characterization*

For the design of the composition in this work, as well as the consideration of MPB based on the phase diagram and preliminary experiment, Goldschmidt's tolerance factor *t* is an important technique to check perovskite structural distortion and the stability of the $ABO_3$ complex oxides as shown below [24]:

$$t = \frac{r_A + r_O}{\sqrt{2}(r_B + r_O)}$$

Using the revised effective ionic radii calculated by Shannon [25], the tolerance factor *t* can be calculated, where the ionic radii of $Pb^{2+}$ in 12-CN (coordination number) is 1.49 Å, $Ni^{2+}$ (6-CN) 0.69 Å, $Ti^{4+}$ (6-CN) 0.605 Å, $Fe^{3+}$ (6-CN, high spin state) 0.645 Å, $Zr^{4+}$ (6-CN) 0.72 Å and $O^{2-}$ (6-CN) 1.4 Å. The dilemma is the ionic radius for $Bi^{3+}$ just having maximum 8-CN with 1.17 Å. Via linear extrapolation of the ionic radius based on the relationship between the ionic radii and the coordination number, the predicted ionic radius for $Bi^{3+}$ with 12-CN would be 2.06 Å. Then, the calculated *t* value range is 0.9643–1.0438 with $Bi^{3+}$ in 8-CN to 12-CN. As the calculated *t* value approaches 1, it reveals the perovskite structure stability of the designed 0.21BNT-0.05BF-0.74PZT composition [24].

The successful design of the composition is further confirmed by XRD measurement as shown in Figure 1. A pure perovskite phase is obtained for all the 0.21BNT-0.05BF-0.74PZT ceramics sintered at relatively low sintering temperatures, and no impurity is detected within the XRD measurement limitation. In the enlarged XRD patterns shown in Figure 1b, it can be clearly seen that the phase structure evolution is induced by increasing the sintering temperature. Within the 2θ degree range of 42–60°, the {200}, {210} and {211} diffraction reflections show broadened singlet-like peaks for the 1010 °C sintered sample, showing a typical MPB composition characteristic [26]. For the 1020–1050 °C sintered ceramics, apparent splitting appears in the above three diffraction peaks accompanied by the change in diffraction peak intensity of the split peaks. The apparent splitting of the {211} diffraction reflection reveals the existence of rhombohedral distortion [26].

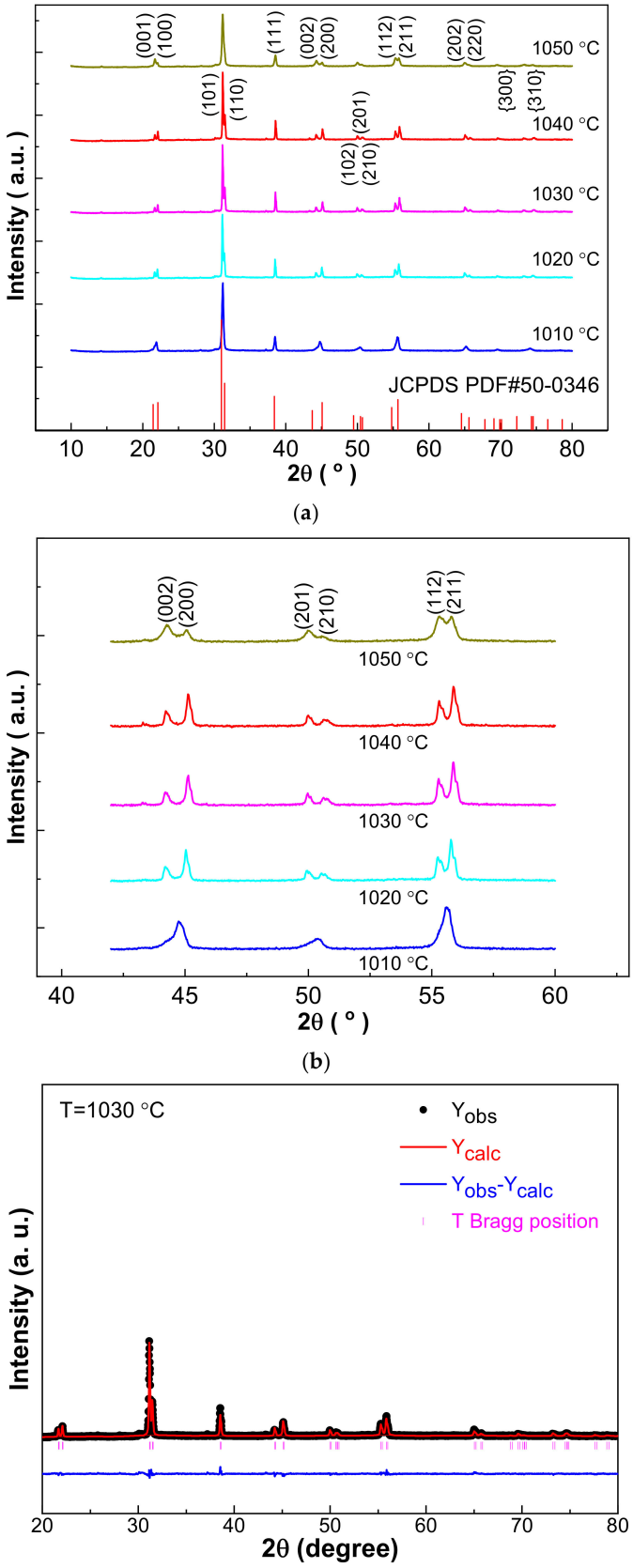


**Figure 1.** (**a**) XRD patterns of low-temperature sintered 0.21BNT-0.05BF-0.74PZT ceramics sintered between 1010 °C and 1050 °C; (**b**) zoomed XRD patterns with 2θ being 42–60°; (**c**) Rietveld refinement of 1030 °C sintered 0.21BNT-0.05BF-0.74PZT ceramics.

Since the major phase shows tetragonal symmetry, the phase structure of the 0.21BNT-0.05BF-0.74PZT ceramics is refined by the Rietveld method and indexed as a tetragonal phase (referred to JCPDS 50-0346). Figure 1c shows XRD Rietveld refinement using the 1030 °C sintered 0.21BNT-0.05BF-0.74PZT ceramics as an example. Based on this, lattice parameters were calculated and are shown in Table 1 combined with refinement parameters. All ceramics have excellent fitting accuracy since all fitting parameters are less than $R_{wp} \leq 6.12\%$, $R_p \leq 4.25\%$, and $\chi^2 \leq 5.770$, showing high reliability of the Rietveld method. Table 2 shows density data, where theoretical density was calculated based on the XRD calculated cell volume and chemical formula weight, and bulk density was measured by Archimedes' water immersion method [21]. The low-temperature sintering technique with the addition of $LiBO_2$ is successful in this work since a large density can be obtained. Within the narrow sintering temperature range, the primary cell volume and relative density present a similar change trend, i.e., increasing first and then decreasing with an increasing sintering temperature. The best ceramics are prepared at a rather low sintering temperature of 1030 °C, and their density is 7.802 g/cm$^3$ and relative density reaches 96.56%, satisfying the production and quality requirements of the electronic ceramic industry. The tetragonality factor c/a also exhibits an increasing first and then decreasing variation affected by sintering temperature, showing the change characteristic of tetragonal distortion [27].

**Table 1.** Lattice constants with P4mm space group and fitting precision parameters of 0.21BNT-0.05BF-0.74PZT ceramics sintered at different temperatures refined by Rietveld method.

| Sintering Temperature (°C) | a = b (Å) | c (Å) | α = β = γ (°) | Reliability Factors |
|---|---|---|---|---|
| 1010 | 4.046819 | 4.071851 | 90 | $R_{wp}$ = 6.12%, $R_p$ = 4.25%, $\chi^2$ = 5.770 |
| 1020 | 4.024786 | 4.091517 | 90 | $R_{wp}$ = 5.56%, $R_p$ = 3.94%, $\chi^2$ = 4.492 |
| 1030 | 4.015606 | 4.091098 | 90 | $R_{wp}$ = 4.84%, $R_p$ = 3.51%, $\chi^2$ = 3.587 |
| 1040 | 4.016916 | 4.090731 | 90 | $R_{wp}$ = 4.82%, $R_p$ = 3.54%, $\chi^2$ = 3.700 |
| 1050 | 4.030802 | 4.094163 | 90 | $R_{wp}$ = 4.16%, $R_p$ = 3.11%, $\chi^2$ = 2.607 |

**Table 2.** Cell volume, density and resistance of low-temperature sintered 0.21BNT-0.05BF-0.74PZT ceramics at several sintering temperatures.

| Sintering Temperature (°C) | Cell Volume (Å$^3$) | Bulk Density (g/cm$^3$) | Theoretical Density (g/cm$^3$) | Relative Density (%) | Resistivity (Ω·cm) |
|---|---|---|---|---|---|
| 1010 | 66.68366 | 7.242 | 8.005032 | 90.46 | $3.56 \times 10^{11}$ |
| 1020 | 66.27808 | 7.677 | 8.043474 | 95.45 | $4.21 \times 10^{11}$ |
| 1030 | 65.96933 | 7.802 | 8.078878 | 96.56 | $6.68 \times 10^{11}$ |
| 1040 | 66.00646 | 7.550 | 8.080214 | 93.45 | $1.22 \times 10^{11}$ |
| 1050 | 66.51936 | 7.258 | 8.016112 | 90.54 | $1.74 \times 10^{11}$ |

### *3.2. SEM Observation*

The largest densification of the 0.21BNT-0.05BF-0.74PZT ceramics sintered at 1030 °C is confirmed in Figure 2 by SEM observation accompanied by the corresponding grain size statistics. The free surface shows an obvious grain boundary, with clear grains and almost without visible pores, consistent with the high density. For the low-temperature sintered ceramics, no other characteristic grains appear, further showing the stability of the perovskite structure obtained in this work. Due to the low-temperature sintering technology, the solid-state sintering mechanism has a major effect in the ceramics' densification process since most grains have a polyhedron shape with a large aspect ratio. The liquid phase sintering mechanism also contributes to the sintering process due to the low melting point of Pb and Bi oxides [18,19], and it produces relatively large grains with an average grain size of 11.74 μm. Due to the utilization of the low-temperature sintering technique, a large grain

size appears in the 0.21BNT-0.05BF-0.74PZT ferroelectric ceramics, which can improve the ceramics' quality and generate an extrinsic contribution to electrical performance [28].

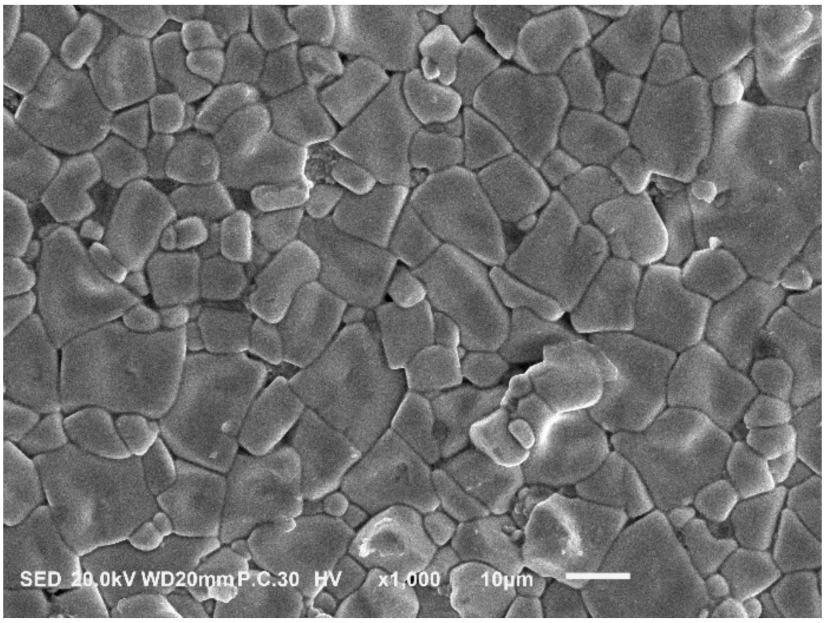


(**a**)

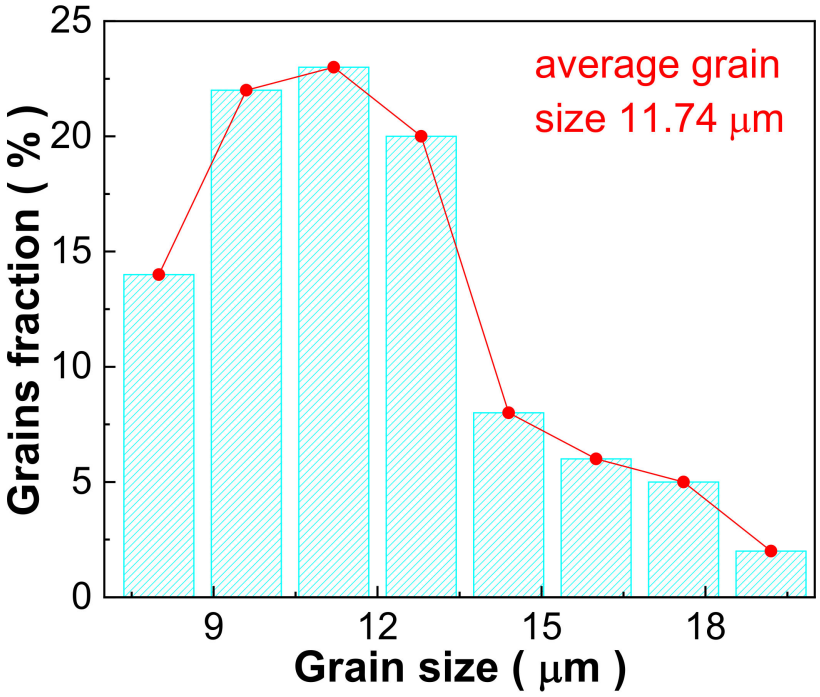


(**b**)

**Figure 2.** SEM image (**a**) and corresponding grain size distribution statistics based on two micrographs (**b**) of 1030 °C sintered 0.21BNT-0.05BF-0.74PZT ceramics.

### *3.3. Resistance and Dielectric Performance*

From Table 2 it can be seen that the resistivity of all of the low-temperature sintered 0.21BNT-0.05BF-0.74PZT ceramics is larger than $10^{11}$ Ω·cm, which is beneficial as it increases the dielectric breakdown strength and obtains large piezoelectricity due to increasing the poling electric field [29]. The resistivity versus the sintering temperature

relationship also presents the largest value at the 1030 °C sintering temperature, which can be attributed to the largest relative density.

The influence of sintering temperature on the dielectric performance of the 0.21BNT-0.05BF-0.74PZT ceramics is shown in Figure 3. All curves present a similar shape, where broad dielectric constant-temperature curves accompanied by a sole wide dielectric peak can be attributed to the relaxor ferroelectric state to paraelectric phase transition. Important dielectric performance parameters are given in Table 3. With the increase in sintering temperature, the dielectric constant peak temperature ($T_m$) increases first and reaches a maximum value of 269 °C at the 1030 °C sintering temperature, and then declines with a variation of 10 °C in $T_m$, whereas the dielectric constant maximum value ($\varepsilon_m$) decreases first, then increases to a maximum value of 16,085.5 at the 1040 °C sintering temperature, and finally decreases again with a variation of 3409.6. Both maximum values appear at different sintering temperatures, which is also considered to relate to the relaxor ferroelectric characteristic [8].

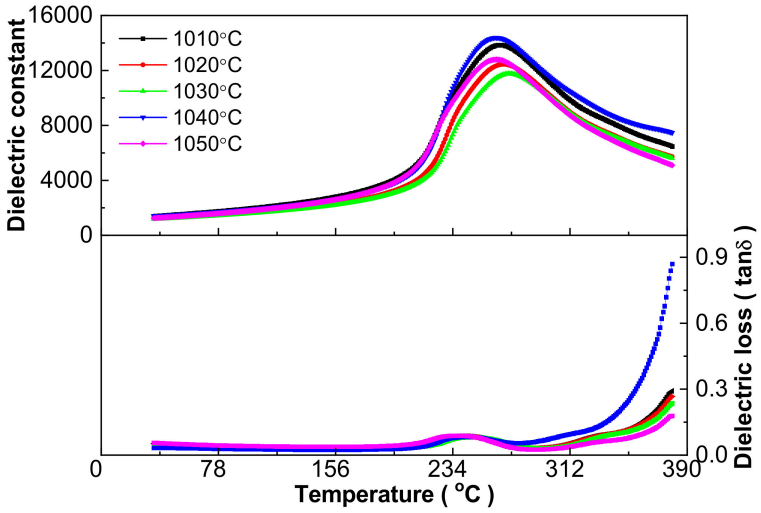


**Figure 3.** Dielectric performance versus temperature relationship at 1 kHz of 0.21BNT-0.05BF-0.74PZT ceramics sintered between 1010 and 1050 °C.

**Table 3.** Important dielectric parameters of 0.21BNT-0.05BF-0.74PZT ceramics sintered at several temperatures.

| Sintering Temperature (°C) | Dielectric Peak Temperature $T_m$ (°C) | Maximum Dielectric Constant ($\varepsilon_m$) | Curie–Weiss Constant (C) | Curie–Weiss Temperature (°C) | $T_{CW}$ (Obey Curie–Weiss Law Temperature) (°C) | Diffuseness Coefficient (γ) |
|---|---|---|---|---|---|---|
| 1010 | 262 | 14,939.8 | $1.277 \times 10^6$ | 266 | 277 | 1.697 |
| 1020 | 265 | 13,435.5 | $1.075 \times 10^6$ | 268 | 281 | 1.705 |
| 1030 | 269 | 12,675.9 | $1.064 \times 10^6$ | 272 | 290 | 1.720 |
| 1040 | 260 | 16,085.5 | $1.064 \times 10^6$ | 266 | 290 | 1.733 |
| 1050 | 259 | 13,782.5 | $8.849 \times 10^5$ | 263 | 290 | 1.698 |

The relaxor behavior is further shown with dielectric performance at different frequencies in Figure 4 using three samples as examples. Actually, all samples have apparent dielectric frequency dispersion, broad dielectric peaks and a diffused phase transition characteristic, i.e., presenting an obvious difference in the $T_m$ and $\varepsilon_m$ values at different frequencies, although detailed values show a difference for the ceramics sintered at different temperatures. Normally, dielectric loss exhibits a more apparent frequency dispersion, and the temperature of the loss tangent (tanδ) extremum value ($T_m'$) is lower than $T_m$ for relaxor ferroelectrics [8]. The difference in the above two temperatures ($T_m$ and $T_m'$) can

be regarded as a signature of the degree of relaxor behavior. The unusual fast increase in dielectric loss above the $T_m$' temperature (Figures 3 and 4) can be attributed to the evaporation of Pb and Bi during sintering, although using the low-temperature sintering technique, which generates point defects, causes thermally activated lossy conduction and leads to an abnormal increase in dielectric loss [30] as shown below [29]:

$$Pb_{Pb}^{\times} + O_O^{\times} \rightarrow Pb\uparrow + \frac{1}{2}O_2\uparrow + V_{Pb}'' + V_O^{\cdot\cdot} \quad (1)$$

$$2Bi_{Bi}^{\times} + 3O_O^{\times} \rightarrow 2Bi\uparrow + \frac{3}{2}O_2\uparrow + 2V_{Bi}''' + 3V_O^{\cdot\cdot} \quad (2)$$

The evaporation of Pb and Bi was detected by energy dispersive X-ray (EDX) measurement as shown in Figures 5, S1 and S2 and Table 4. Since the free surface of ceramics was used for the EDX measurement and the sample was thermally etched at 800 °C for 30 min, the atomic percentage of all metal elements was far less than the designed composition. Such a difference can be used to reveal the evaporation of metal elements, especially for Bi and Pb, during the sintering process. Although the evaporation of some metals during sintering is inevitable, the distribution of metal elements is rather homogeneous as shown in Figure S2, where the grain boundary presents higher sublimation capability due to the amorphous state or disordered arrangement of atoms [19].

**Table 4.** Element type and corresponding atomic percentage of 1030 °C sintered 0.21BNT-0.05BF-0.74PZT ceramics measured at different locations.

| Element | Atom% (Location 1) | Atom% (Location 2) | Atom% (Location 3) |
|---|---|---|---|
| Bi | 8.73 ± 0.07 | 8.82 ± 0.07 | 9.53 ± 0.07 |
| Ni | 3.26 ± 0.02 | 2.18 ± 0.02 | 3.47 ± 0.02 |
| Ti | 11.22 ± 0.01 | 11.31 ± 0.01 | 11.94 ± 0.02 |
| Fe | 1.90 ± 0.01 | 1.70 ± 0.01 | 2.07 ± 0.01 |
| Pb | 19.05 ± 0.07 | 19.27 ± 0.07 | 19.76 ± 0.07 |
| Zr | 8.42 ± 0.03 | 9.19 ± 0.03 | 8.51 ± 0.03 |
| O | 47.42 ± 0.02 | 47.53 ± 0.02 | 44.71 ± 0.02 |

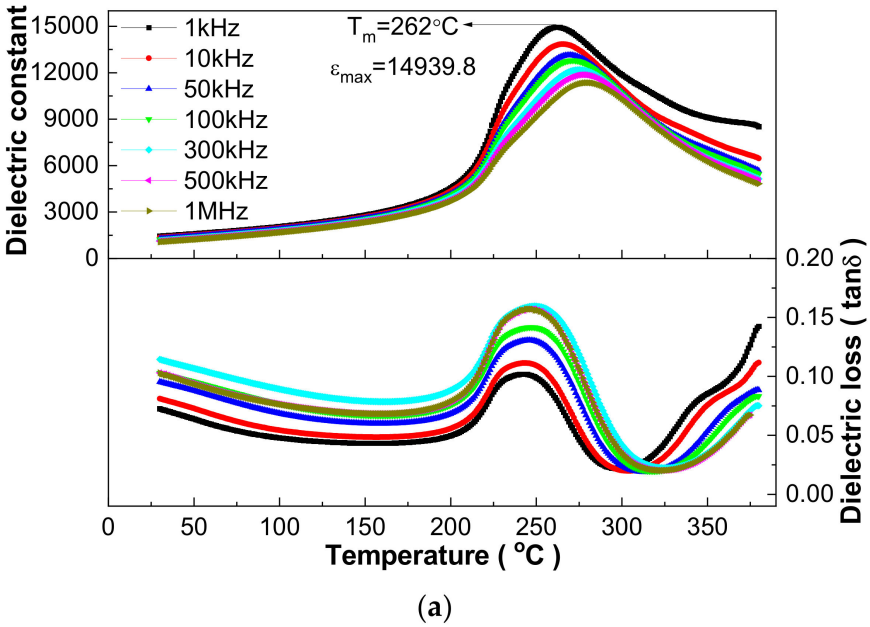


(**a**)

**Figure 4.** *Cont.*

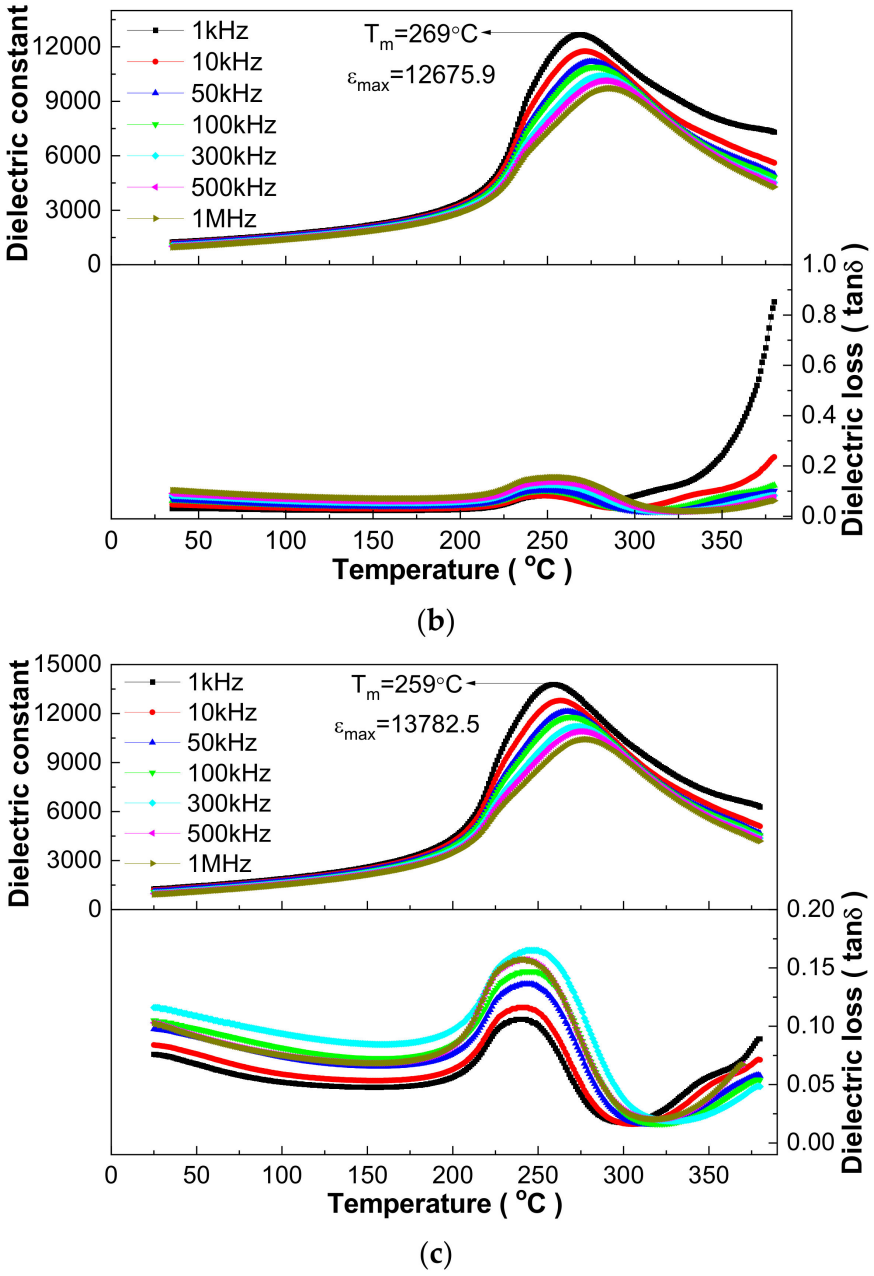


**Figure 4.** Typical dielectric performance–temperature curves measured at several frequencies upon heating of 0.21BNT-0.05BF-0.74PZT ceramics sintered at (**a**) 1010 °C; (**b**) 1030 °C and (**c**) 1050 °C.

Dielectric response fitting using dielectric data above the $T_m$ temperature provides an effective way to discriminate ferroelectrics' type. Using the 1030 °C sintered 0.21BNT-0.05BF-0.74PZT ceramics as an example, the fitted Curie–Weiss law is $\varepsilon = 1.064 \times 10^6/(T - 272)$ and the fitted exponential law is $1/\varepsilon - 1/10897.5 = (T - 277)^{1.720}/(2.10 \times 10^7)$ (Figure 6) [31,32]. Combined with the data shown in Table 3, the fitted Curie–Weiss constant C of all samples has $10^5$ magnitude order. Moreover, the C value presents a decreasing trend, the Curie–Weiss temperature increases first and then decreases, and the temperature above which the Curie–Weiss law can be obeyed ($T_{CW}$) shows an increasing trend with increasing sintering temperature, i.e., the temperature difference of $T_{CW}$-$T_m$ is 11–27 °C for different samples. The fitted diffused coefficient γ increases first and reaches a maximum value of 1.733 for the 1040 °C sintered 0.21BNT-0.05BF-0.74PZT ceramics, and then decreases slightly, revealing the change in the relaxation characteristic degree. All the fitted γ values are larger than 1.69 but less than 2. Based on these results, the 0.21BNT-0.05BF-0.74PZT samples

present complicated dielectric response behavior, and can be regarded as displacive driven ferroelectric phase transition superimposed on obvious frequency dispersion [32]. Such a phase transition characteristic is normally related to the generation of polar nano-regions (PNRs) caused by local nano-sized nonuniformity of chemical composition, disordered distribution of cations at the A-site and B-site of the perovskite structure [33], and a randomly distributed strain field and electric field [34].

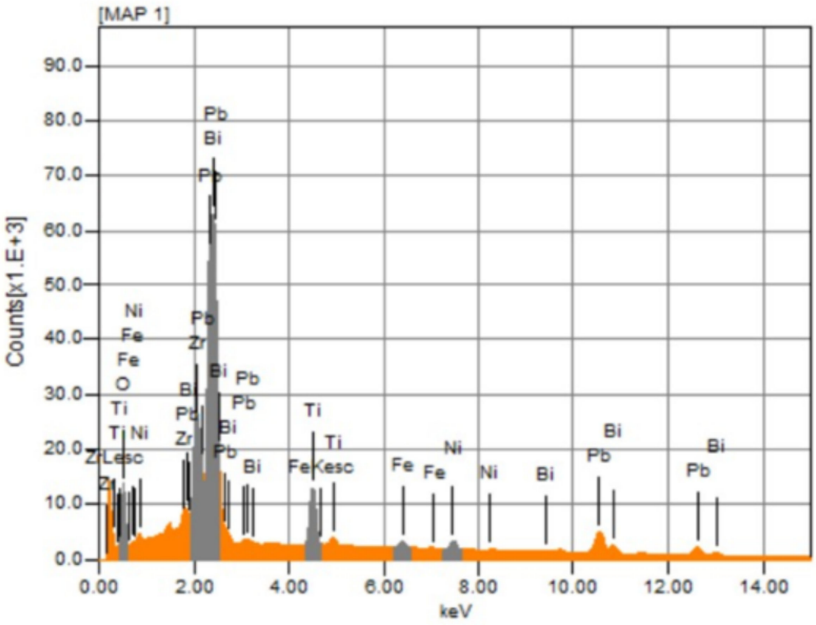


**Figure 5.** Typical EDX spectrum of 1030 °C sintered 0.21BNT-0.05BF-0.74PZT ceramics.

Vogel–Fulcher fitting provides another technique to research relaxation characteristic as shown in Figure 7, also using the 1030 °C sintered 0.21BNT-0.05BF-0.74PZT ceramics as an example. Based on the Vogel–Fulcher formula, $f = f_0 \exp[E_a/k_B(T - T_{VF})]$, the fitting uses 1–1000 kHz data; therefore, the empirical relaxation strength $\Delta T_{res} = T_{m(1000\ kHz)} - T_{m(1\ kHz)}$ can be used to describe the frequency dispersion degree [34]. The fitted parameters are $f_0 = 2.62 \times 10^6$ Hz, $E_a = 0.00301$ eV, $T_{VF} = 537$ K and $\Delta T_{res} = 17$ K, respectively, presenting the appearance of composition-induced relaxor-like ferroelectrics. The average activation energy $E_a = 0.00301$ eV is comparable with the thermal excitation energy of kT, reflecting that the dipoles' polarization orientation relates to the thermal excitation process [34]. The fitted Debye frequency $f_0 = 2.62 \times 10^6$ Hz is comparable to that of the $Ba(Zr_{0.30}Ti_{0.70})O_3$ ceramics, correlating with the complex microstructure and the generated point defects due to the evaporation of Pb and Bi during sintering [34].

### *3.4. Piezoelectric Performance*

Figure 8 shows the piezoelectric performance of the 0.21BNT-0.05BF-0.74PZT samples. With the increase in the poling electric field, piezoelectric constant $d_{33}$ increases rapidly, correlating with the easy switching of 180° domains under a high external electric field [5]. With the elevation of the sintering temperature, the $d_{33}$ value increases first and then decreases. The 1030 °C sintered 0.21BNT-0.05BF-0.74PZT ceramics have the largest $d_{33}$ value, being 213.4 pC/N, which is rather large considering the high $T_m$ temperature. The 1030 °C sintered 0.21BNT-0.05BF-0.74PZT ceramics present explicit resonant and anti-resonant shape behavior poled at 25 kV/cm, whereas the maximum phase degree θ is just 34°, showing the possibility of increasing the poling electric field but constrained by the leakage current of the samples. Such a low θ value accompanied from the beginning by a rather low minus θ degree, i.e., nearly −90°, is usually observed in the $(K_{1-x}Na_x)NbO_3$-based lead-free piezoelectric ceramics, and the reason is difficult to explain [35]. Based on the resonant spectra, the mechanical quality factor $Q_m$ and electromechanical coupling

coefficient $K_p$ were calculated and are shown in Table 5. The 0.21BNT-0.05BF-0.74PZT ceramics exhibit an apparent soft piezoelectric materials characteristic due to the existence of a large quantity of point defects as discussed in defect Equations (1) and (2). Overall, the 1030 °C sintered 0.21BNT-0.05BF-0.74PZT ceramics have excellent electrical properties, where $d_{33}$ = 213.4 pC/N, $K_p$ = 37.7% and $Q_m$ = 27.3.

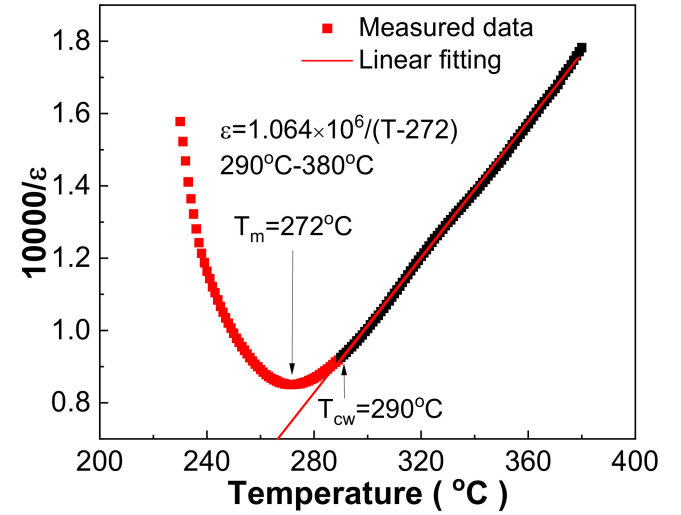


(**a**)

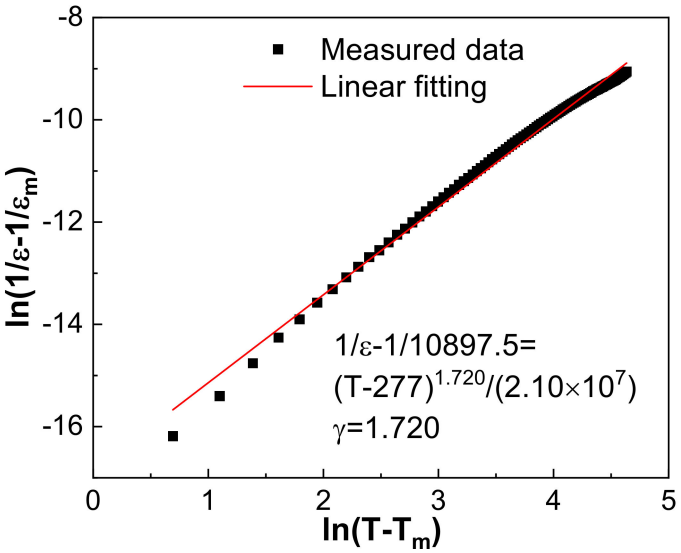


(**b**)

**Figure 6.** Dielectric response fitting of 1030 °C sintered 0.21BNT-0.05BF-0.74PZT ceramics using 10 kHz data. (**a**) Curie–Weiss law; (**b**) quadratic law.

**Table 5.** $K_p$ and $Q_m$ values of 0.21BNT-0.05BF-0.74PZT ceramics sintered at different temperatures poled under 25 kV/cm.

| Sintering Temperature (°C) | $K_p$ (%) | $Q_m$ |
|---|---|---|
| 1010 | 30.4 | 13.3 |
| 1020 | 30.5 | 15.4 |
| 1030 | 37.7 | 27.3 |
| 1040 | 32.3 | 14.3 |
| 1050 | 37.3 | 19.5 |

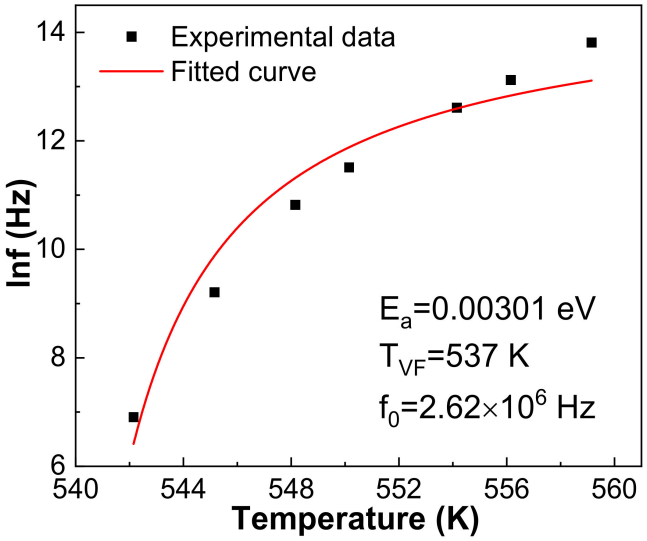


**Figure 7.** Vogel–Fulcher fitting of 1030 °C sintered 0.21BNT-0.05BF-0.74PZT sample.

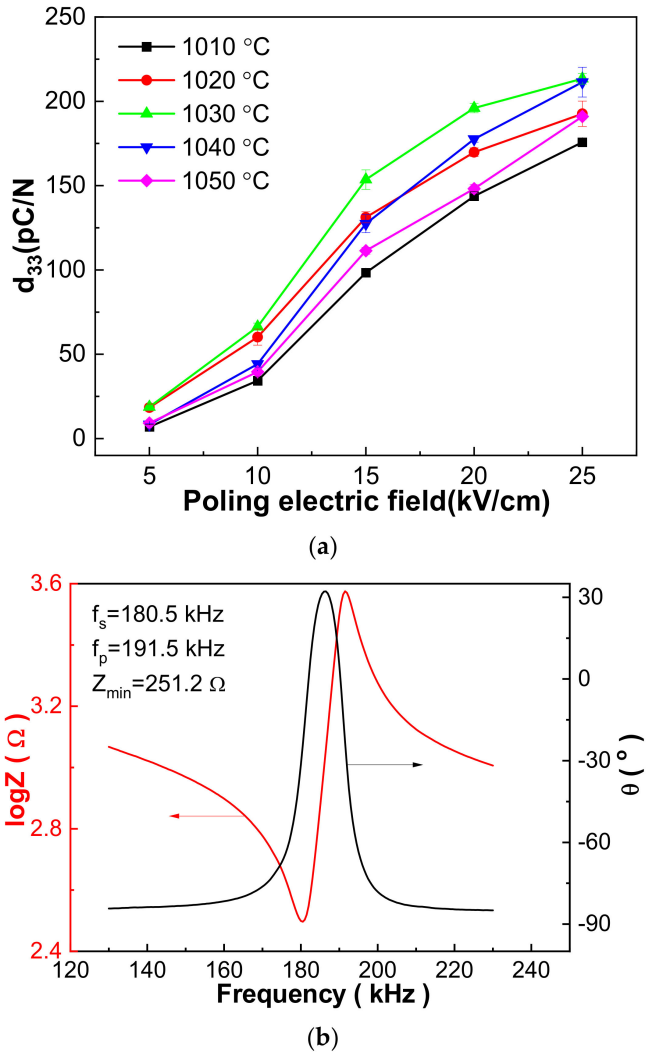


**Figure 8.** (**a**) Poling electric-field-dependent piezoelectricity $d_{33}$ of 0.21BNT-0.05BF-0.74PZT samples sintered at different temperatures; (**b**) impedance and phase degree versus frequency curves of 1030 °C sintered 0.21BNT-0.05BF-0.74PZT ceramics poled at 25 kV/cm.

### *3.5. Conduction Mechanism*

The impedance spectra and conduction mechanism were studied using the 1030 °C sintered 0.21BNT-0.05BF-0.74PZT ceramics as an example. The real part of impedance Z′ tends to decrease sharply before a certain frequency and then becomes stable, and the imaginary part of impedance Z″ normally presents a peak with the increase in frequency. With the increase in measurement temperature, both the Z′ and Z″ impedance values decrease, the Z″ peak frequency moves to a high frequency and the Z″ peak broadens obviously.

Figure 9 shows Cole–Cole-like Z′-Z″ relationship curves based on the impedance measurement. At lower temperatures, the curves exhibit a straight line shape, whereas perfect Cole–Cole-shaped semi-circles are obtained at higher temperatures. The curve at different temperatures just presents a sole semi-circle, revealing the contribution of the grains' conduction, and correlating with the thermally activated conduction of point defects generated as shown in defect Equations (1) and (2) [36].

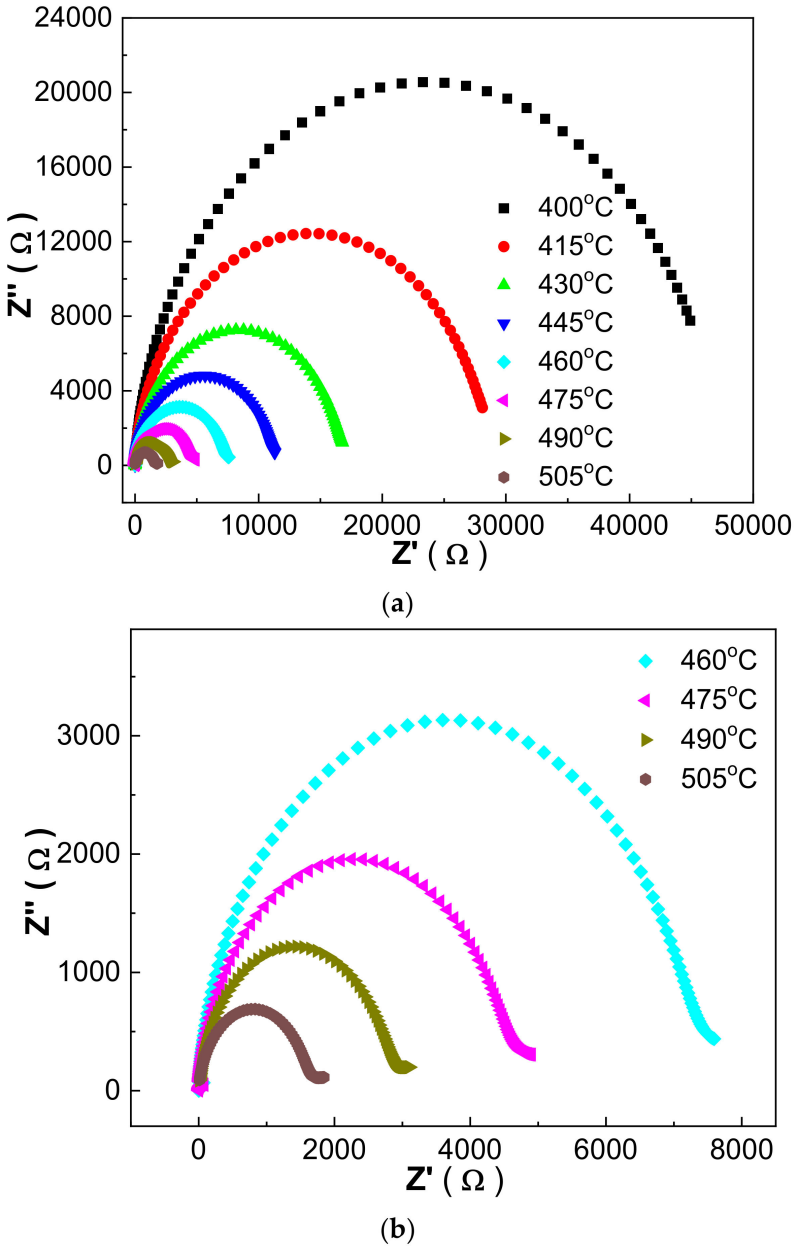


**Figure 9.** (**a**) Cole–Cole impedance spectra of 1030 °C sintered 0.21BNT-0.05BF-0.74PZT ceramics measured within 400–505 °C; (**b**) enlarged Cole–Cole impedance spectra measured within 460–505 °C.

To reveal the type of point defects, the high-temperature conductivity was linearly fitting according to the Arrhenius law, based on which, the activation energy $E_a$ of the sample was calculated and the point defects' type could be determined. The sample's conductivity was extrapolated from impedance spectra via formula $\sigma = t/RS$, in which t is the thickness of the sample, S is the sample's area and R is the real part of the impedance at low frequencies. The calculated conductivity and liner fitting result are shown in Figure 10, where the fitting line matches well with the extrapolated data and shows the reliability of the Arrhenius law fitting. The fitted $E_a$ = 1.21 eV, approaching close to 1 eV, shows that the oxygen vacancies produced by the evaporation of Pb and Bi during sintering as discussed in defect Equations (1) and (2) dominate the conduction process in the 0.21BNT-0.05BF-0.74PZT ceramics at high temperatures [37].

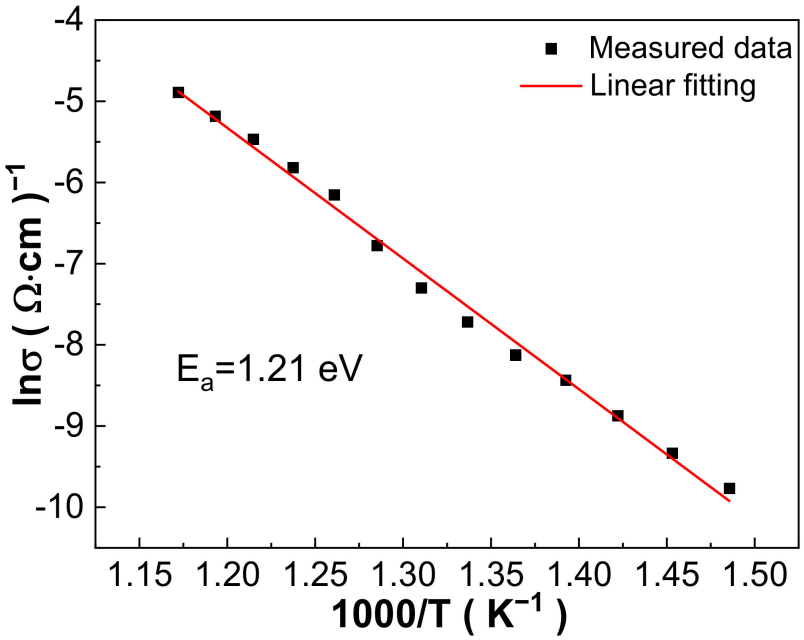


**Figure 10.** Conductivity–temperature relationship of 1030 °C sintered 0.21BNT-0.05BF-0.74PZT ceramics.

## 4. Conclusions

Pure perovskite 0.21BNT-0.05BF-0.74PZT ceramics were prepared by low-temperature sintering technology, which presents a narrow sintering temperature range, and the tetragonal distortion c/a increases first and then decreases with the increasing sintering temperature. Within the narrow sintering temperature range, the primary cell volume and relative density present parabolic curve-like change, and the best ceramics are prepared at a low sintering temperature of 1030 °C accompanied by large densification of 96.56% and rather uniform micromorphology. All of the sintered 0.21BNT-0.05BF-0.74PZT ceramics have resistivity larger than $10^{11}$ Ω·cm and excellent dielectric properties, where the highest $T_m$ 269 °C and largest $\varepsilon_m$ 16,085.5 are acquired at 1030 °C and 1040 °C sintering temperatures, respectively. The relaxation characteristic is confirmed by exponential law dielectric response fitting and Vogel–Fulcher fitting combined with dielectric frequency dispersion and diffused phase transition. The 1030 °C sintered 0.21BNT-0.05BF-0.74PZT ceramics have excellent electrical properties, in which $T_m$ = 269 °C, $d_{33}$ = 213.4 pC/N, $K_p$ = 37.7% and $Q_m$ = 27.3. Oxygen vacancies produced due to the evaporation of Bi and Pb during sintering revealed by the EDX measurement perform a control function in the high-temperature grains' conduction. The rather large piezoelectricity combined with a relatively high $T_m$ temperature provides the prospect of their application in harsh operation temperature fields for the 0.21BNT-0.05BF-0.74PZT ceramics studied.

**Supplementary Materials:** The following supporting information can be downloaded at: https://www.mdpi.com/article/10.3390/ma16093459/s1, Figure S1: EDX spectra of 1030 °C sintered 0.21BNT-0.05BF-0.74PZT ceramics at different locations; Figure S2: Element surface mapping of 1030 °C sintered 0.21BNT-0.05BF-0.74PZT ceramics at different locations.

**Author Contributions:** Conceptualization, B.F.; Supervision, B.F.; Methodology, J.S.; Formal analysis, S.W. and Q.W.; Investigation, W.W., S.W., J.S. and Q.W.; Data curation, W.W. and S.W.; Writing—original draft, S.W. and W.W.; Writing—review & editing, B.F. All authors have read and agreed to the published version of the manuscript.

**Funding:** The authors thank the Top-notch Academic Programs Project of Jiangsu Higher Education Institutions and the Priority Academic Program Development of Jiangsu Higher Education Institutions for their financial support.

**Institutional Review Board Statement:** Not applicable.

**Informed Consent Statement:** Not applicable.

**Data Availability Statement:** All data that support the findings of this study are included within the article and Supplementary File.

**Conflicts of Interest:** The authors declare that they have no known competing financial interests or personal relationships that could have appeared to influence the work reported in this paper.

## References

1. Damjanovic, D. Materials for high temperature piezoelectric transducers. *Curr. Opin. Solid State Mater. Sci.* **1998**, *3*, 469–473. [CrossRef]
2. Gao, Z.; Lu, C.; Wang, Y.; Yang, S.; Yu, Y.; He, H. Super stable ferroelectrics with high Curie point. *Sci. Rep.* **2016**, *6*, 24139. [CrossRef] [PubMed]
3. Wang, Y.; Ma, H.; Yuan, G.; Luo, H.; Viehland, D. Heterogeneous domain configurations in ferroelectric crystals during thermal depolarization. *J. Am. Ceram. Soc.* **2017**, *100*, 1751–1759. [CrossRef]
4. Hao, J.; Li, W.; Zhai, J.; Chen, H. Progress in high-strain perovskite piezoelectric ceramics. *Mater. Sci. Eng. R* **2019**, *135*, 1–57. [CrossRef]
5. Ji, W.; Fang, B.; Zhao, X.; Zhang, S.; Lu, X.; Ding, J. Enhancing electrical properties of high-Curie temperature piezoelectric ceramics BNT-PZT and their mechanism. *Curr. Appl. Phys.* **2019**, *19*, 1367–1373. [CrossRef]
6. Chen, L.; Liu, H.; Qi, H.; Chen, J. High-electromechanical performance for high-power piezoelectric applications: Fundamental, progress, and perspective. *Prog. Mater. Sci.* **2022**, *127*, 100944. [CrossRef]
7. Li, F.; Lin, D.B.; Chen, Z.B.; Cheng, Z.X.; Wang, J.L.; Li, C.C.; Xu, Z.; Huang, Q.W.; Liao, X.Z.; Chen, L.Q.; et al. Ultrahigh piezoelectricity in ferroelectric ceramics by design. *Nat. Mater.* **2018**, *17*, 349–356. [CrossRef]
8. Lin, D.; Zhang, S.; Gorzkowski, E.; Zhou, S.; Liu, W.; Li, F. Investigation of morphotropic phase boundaries in PIN-PSN-PT relaxor ferroelectric ternary systems with high $T_{r-t}$ and $T_c$ phase transition temperatures. *J. Eur. Ceram. Soc.* **2017**, *37*, 2813–2823. [CrossRef]
9. Sato, Y.; Hirayama, T.; Ikuhara, Y. Monoclinic nanodomains in morphotropic phase boundary $Pb(Mg_{1/3}Nb_{2/3})O_3$-$PbTiO_3$. *App. Phys. Lett.* **2014**, *104*, 082905. [CrossRef]
10. Zhu, R.; Fang, B.; Zhang, S.; Lu, X.; Ding, J. Composition design of PMN-PH-PT piezoelectric ceramics for high-temperature actuator applications. *Mater. Res. Express* **2020**, *7*, 046304. [CrossRef]
11. Eitel, R.E.; Randall, C.A.; Shrout, T.R.; Rehrig, P.W.; Hackenberger, W.; Park, S.-E. New high temperature morphotropic phase boundary piezoelectrics based on $Bi(Me)O_3$-$PbTiO_3$ ceramics. *Jpn. J. Appl. Phys.* **2001**, *40*, 5999–6002. [CrossRef]
12. Wei, Y.; Bai, C.; Jin, C.; Zhu, W.; Jian, Z.; Nan, R.; Hu, L.; Dai, Z. Super short-range magnetic orderings in a multiferroic relaxor ceramic $0.41Bi(Ni_{1/2}Zr_{1/2})O_3$-$0.59PbTiO_3$. *J. Mater. Sci.* **2021**, *56*, 11838–11846. [CrossRef]
13. Choi, S.M.; Stringer, C.J.; Shrout, T.R.; Randall, C.A. Structure and property investigation of a Bi-based perovskite solid solution: $(1-x)Bi(Ni_{1/2}Ti_{1/2})O_3$-$xPbTiO_3$. *J. Appl. Phys.* **2005**, *98*, 034108. [CrossRef]
14. Zhao, T.; Fei, C.; Pu, K.; Dai, X.; Song, J.; Wang, C.; Dong, S. Structure evolution and enhanced electrical performance for $BiScO_3$-$Bi(Ni_{1/2}Zr_{1/2})O_3$-$PbTiO_3$ solid solutions near the morphotropic phase boundary. *J. Alloys Compd.* **2021**, *873*, 159844. [CrossRef]
15. Ansell, T.Y.; Cann, D.P.; Sapper, E.; Rödel, J. Thermal depolarization in the high-temperature ternary piezoelectric system $xPbTiO_3$-$yBiScO_3$-$zBi(Ni_{1/2}Ti_{1/2})O_3$. *J. Am. Ceram. Soc.* **2015**, *98*, 455–463. [CrossRef]
16. Ji, W.; Feng, S.; Fang, B.; Zhao, X.; Zhang, S.; Ding, J.; Luo, H. Facile preparation and performance of novel high-$T_C$ $xBi(Ni_{1/2}Ti_{1/2})O_3$-$(1-x)Pb(Zr_{1/2}Ti_{1/2})O_3$ piezoceramics. *Curr. Appl. Phys.* **2018**, *18*, 289–296. [CrossRef]
17. Zhai, L.; Shi, Y.G.; Gao, J.L.; Tang, S.L.; Du, Y.W. Ferroelectric and magnetic properties in high-pressure synthesized $BiFeO_3$ compound. *J. Alloys Compd.* **2011**, *509*, 7591–7594. [CrossRef]

18. Sun, X.; Chen, J.; Yu, R.; Xing, X.; Qiao, L.; Liu, G. $BiFeO_3$-doped $(Na_{0.5}K_{0.5})NbO_3$ lead-free piezoelectric ceramics. *Sci. Technol. Adv. Mater.* **2008**, *9*, 025004. [CrossRef]
19. Luo, F.; Guan, H.W.; Peng, R.; Jian, J.; Chen, J.G.; Cheng, J.R. Low-temperature sintering of BF-PT-BZ ternary solid solutions with enhanced piezoelectric properties. *J. Am. Ceram. Soc.* **2019**, *102*, 5958–5965. [CrossRef]
20. Beuerlein, M.A.; Kumar, N.; Usher, T.-M.; Brown-Shaklee, H.J.; Raengthon, N.; Reaney, I.M.; Cann, D.P.; Jones, J.L.; Brennecka, G.L. Current understanding of structure-processing-property relationships in $BaTiO_3$-$Bi(M)O_3$ dielectrics. *J. Am. Ceram. Soc.* **2016**, *99*, 2849–2870. [CrossRef]
21. Wang, S.; Fang, B.; Zhao, X.; Zhang, S.; Lu, X.; Ding, J. Phase formation and performance of high Curie temperature $Bi(Ni_{0.5}Ti_{0.5})O_3$-$BiFeO_3$-$PbTiO_3$ ceramics. *Ferroelectrics* **2022**, *600*, 105–123. [CrossRef]
22. Chandrakala, E.; Praveen, J.P.; Hazra, B.K.; Das, D. Effect of sintering temperature on structural, dielectric, piezoelectric and ferroelectric properties of sol-gel derived BZT-BCT ceramics. *Ceram. Int.* **2016**, *42*, 4964–4977. [CrossRef]
23. Ying, Y.; Xiong, X.; Wang, N.; Zheng, J.; Yu, J.; Li, W.; Qiao, L.; Cai, W.; Li, J.; Huang, H.; et al. Low temperature sintered MnZn ferrites for power applications at the frequency of 1 MHz. *J. Eur. Ceram. Soc.* **2021**, *41*, 5924–5930. [CrossRef]
24. Lee, W.-C.; Huang, C.-Y.; Tsao, L.-K.; Wu, Y.-C. Chemical composition and tolerance factor at the morphotropic phase boundary in $(Bi_{0.5}Na_{0.5})TiO_3$-based piezoelectric ceramics. *J. Eur. Ceram. Soc.* **2009**, *29*, 1443–1448. [CrossRef]
25. Shannon, R.D. Revised effective ionic radii and systematic studies of interatomic distances in Halides and chalcogenides. *Acta Cryst.* **1976**, *A32*, 751–766. [CrossRef]
26. Yang, Y.; Liu, C.; Ji, Y.; He, L.; Ren, X. Designed morphotropic relaxor boundary ceramic exhibiting large electrostrain and negligible hysteresis. *Acta Mater.* **2021**, *208*, 116720. [CrossRef]
27. Bhattacharjee, S.; Pande, D. Effect of stress induced monoclinic to tetragonal phase transformation in the multiferroic $(1-x)BiFeO_3$-$xPbTiO_3$ system on the width of the morphotropic phase boundary and the tetragonality. *J. Appl. Phys.* **2011**, *110*, 084105. [CrossRef]
28. Tutuncu, G.; Fan, L.; Chen, J.; Xing, X.; Jones, J.L. Extensive domain wall motion and deaging resistance in morphotropic $0.55Bi(Ni_{1/2}Ti_{1/2})O_3$-$0.45PbTiO_3$ polycrystalline ferroelectrics. *Appl. Phys. Lett.* **2014**, *104*, 132907. [CrossRef]
29. Yang, Y.; Wang, H.; Bi, L.; Zheng, Q.; Fan, G.; Jie, W.; Lin, D. High energy storage density and discharging efficiency in $La^{3+}/Nb^{5+}$ co-substituted $(Bi_{0.5}Na_{0.5})_{0.94}Ba_{0.06}TiO_3$ ceramics. *J. Eur. Ceram. Soc.* **2019**, *39*, 3051–3056. [CrossRef]
30. Wang, Y.; Jie, W.; Yang, C.; Wei, X.; Hao, J. Colossal permittivity materials as superior dielectrics for diverse applications. *Adv. Funct. Mater.* **2019**, *29*, 1808118. [CrossRef]
31. Uchino, K.; Nomura, S. Critical exponents of the dielectric constants in diffused-phase-transition crystals. *Ferroelectr. Lett.* **1982**, *44*, 55–61. [CrossRef]
32. Wei, X.; Feng, Y.; Yao, X. Dielectric relaxation behavior in barium stannate titanate ferroelectric ceramics with diffused phase transition. *Appl. Phys. Lett.* **2003**, *83*, 2031–2033.
33. Shvartsman, V.V.; Kleemann, W.; Dec, J.; Xu, Z.; Lu, K.S.G. Diffuse phase transition in $BaTi_{1-x}Sn_xO_3$ ceramics: An intermediate state between ferroelectric and relaxor behavior. *J. Appl. Phys.* **2006**, *99*, 124111. [CrossRef]
34. Tang, X.G.; Chew, K.-H.; Chan, H.L.W. Diffuse phase transition and dielectric tunability of $Ba(Zr_yTi_{1-y})O_3$ relaxor ferroelectric ceramics. *Acta Mater.* **2004**, *52*, 5177–5183. [CrossRef]
35. Zhou, Y.; Fang, B.; Zhang, S.; Lu, X.; Ding, J. Enhancing densification and electrical properties of KNN-based lead-free ceramics via two-step sintering. *J. Korean Ceram. Soc.* **2022**, *59*, 551–564. [CrossRef]
36. Bhadauria, P.P.S.; Kolte, J. Impedance and AC conductivity analysis of La-substituted $0.67BiFeO_3$-$0.33BaTiO_3$ solid solution. *Appl. Phys. A* **2022**, *128*, 465. [CrossRef]
37. Pastor, M.; Bajpai, P.K.; Choudhary, R.N. Structural and electrical impedance study of $Pb(Sr_{1/3}Nb_{2/3})O_3$. *J. Phys. Chem. Solids* **2007**, *68*, 1914–1920. [CrossRef]